JOURNAL OF OPTOELECTRONICS AND ADVANCED MATERIALS Vol. 9, No. 1, January 2007, p. 77 - 83

Invited Lecture

Luminescence, quasi-Fermi levels and applied voltage in ideal and real semiconductor structures

R. BRÜGGEMANN, J. BEHRENDS, S. MEIER, S. TARDON
Institut für Physik, Carl von Ossietzky Universität Oldenburg, D-26111 Oldenburg, Germany

We apply Kirchhoff's generalised law for the analysis of the luminescence from crystalline silicon structures. We demonstrate its validity for crystalline silicon by the comparison between experimental and theoretical photoluminescence and electroluminescence spectra for different temperatures and different sample geometries. The band-to-band recombination coefficient, determined from photoluminescence results, decreases slightly above room-temperature with increasing temperature. The electroluminescence efficiency also decreases with increasing temperature and depends strongly on the saturation current density of the silicon diode. The absorptivity term in Kirchoff's generalised law determines both the shape and the height of the luminescence spectra. Transfer of the ideal-diode concept, in which the quasi-Fermi level splitting is directly related to the applied voltage, to real semiconductor *pn* diodes leads to erroneous conclusions. Especially at lower voltages, the quasi-Fermi level splitting can be much larger than expected from the applied voltage.

(Received November 28, 2006; accepted December 21, 2006)

Keywords: Crystalline silicon, Band-to-band recombination coefficient, Quasi-Fermi level, Photoluminescence, Electroluminescence

1. Introduction

Lasher and Stern [1] described the theory for band-to-band recombination between conduction-band electrons and valence-band holes for which the occupation is described by quasi-Fermi levels, ε_{Fn} and ε_{Fp}. The spontaneous radiative recombination rate per energy interval is given by

$$dr_{spont}(\hbar\omega) = \frac{n_r^2(\hbar\omega)^2}{\pi^2\hbar^3c_0^2}\frac{\alpha(\hbar\omega)\mathrm{d}\hbar\omega}{\exp\left(\frac{\hbar\omega-(\varepsilon_{Fn}-\varepsilon_{Fp})}{kT}\right)-1} \quad (1)$$

where n_r is the refractive index, c_0 the vacuum light velocity, α is the absorption coefficient and k is the Boltzmann constant. The emitted luminescence was analysed by Stephens [2] for a finite sample structure and taking into account surface recombination of minority carriers. Würfel [3] formulated that the emitted photon flux per energy interval and solid angle is given by

$$\mathrm{d}j_\gamma(\hbar\omega) = \frac{(\hbar\omega)^2}{4\pi^3\hbar^3c_0^2}\frac{A(\hbar\omega)\mathrm{d}\Omega\mathrm{d}\hbar\omega}{\exp\left(\frac{\hbar\omega-(\varepsilon_{Fn}-\varepsilon_{Fp})}{kT}\right)-1} \quad (2)$$

where A is the absorptivity of the sample and the assumption has been made that the quasi-Fermi levels are spatially constant. This equation may be regarded as Kirchhoff's generalised law.

For non-homogeneous carrier distributions and a non-constant quasi-Fermi level splitting a more complicated version of Eq. (2) involves an integral term to take into account the non-homogeneous generation and propagation of the luminescence photons [4].

For photovoltaic materials, Eq. (2) is important. The quasi-Fermi level splitting $\varepsilon_{Fn} - \varepsilon_{Fp}$ is related to the open-circuit voltage V_{oc} of a solar cell fabricated from this material. Under certain conditions, the achievable V_{oc} may thus be predicted from $\varepsilon_{Fn} - \varepsilon_{Fp}$, determined from a quantitative photoluminescence measurement [3].

Experimental evidence for Kirchhoff's generalised law has been given for direct [3] and indirect semiconductors [4,5]. While excellent agreement was achieved at 300 K between the experimental and analytical photoluminescence spectra for a crystalline silicon wafer [4], some spectral mismatch was observed for a silicon diode solar cell, despite good general agreement [5].

In this paper, we exploit Kirchhoff's generalised law for the analysis of the luminescence of crystalline silicon (c-Si) and we support the validation of Kirchhoff's generalised law for indirect semiconductors, by the comparison of the experimental and analytical luminescence spectra of c-Si in a wide temperature range and for wafer and diode structures with different optical interface conditions for emitted photons. We exploit the relation between the photoluminescence (PL) and the excess carrier densities to determine the band-to-band recombination coefficient in c-Si for temperatures 300 K ≤ T ≤ 393 K, i.e., in a likely operating range for devices like solar cells or light-emitting diodes. We also apply Eq. (2) to the analysis of the electroluminescence (EL) of silicon diodes.

In the last section, we study the transfer of concepts from ideal to real diode applications. For an ideal diode with ideal transport properties of the charge carriers, $\varepsilon_{Fn} - \varepsilon_{Fp} = \mathrm{e}\ V_a$, where V_a is the applied voltage. This relation, together with Eq. (2), has also been applied in solar cell efficiency calculations [6] and is taken to hold in real solar cells [7]. The assumption will critically be discussed here by diode analysis and numerical modelling.

2. Theoretical background

2.1. Kirchoff's generalised law

In many practical cases, Eq. (2) reads

$$\mathrm{d}j_\gamma(\hbar\omega) = \frac{(\hbar\omega)^2}{4\pi^3\hbar^3c_0^2} A(\hbar\omega)\exp\left(-\frac{\hbar\omega}{kT}\right)\exp\left(\frac{\varepsilon_{Fn}-\varepsilon_{Fp}}{kT}\right)\mathrm{d}\Omega\mathrm{d}\hbar\omega \tag{3}$$

because the 1 in the numerator in Eq. (2) can be neglected. The spectral shape of the emitted radiation is thus mainly determined by the product of an energy-dependent Boltzmann term and the absorptivity of the sample structure under study.

2.2. Absorption coefficient

Lucovsky *et al.* [8] determined the relative absorption coefficient from the low-energy range of the PL of GaAs, because α is proportional to the product A/d where d is the sample thickness. Taking full account of the absorptivity, the absorption coefficient was determined by Daub and Würfel [9] over a wide energy range towards very low values of α.

The absorptivity can be determined from the luminescence according to (Eq. (2))

$$A(\hbar\omega) = \frac{\mathrm{d}j_\gamma}{\mathrm{d}\Omega\mathrm{d}\hbar\omega}\frac{4\pi^3\hbar^3c_0^2}{(\hbar\omega)^2}\times \left[\exp\left(\frac{\hbar\omega-(\varepsilon_{Fn}-\varepsilon_{Fp})}{kT}\right)-1\right], \tag{4}$$

provided the quasi-Fermi level splitting is known or A can be matched at sufficiently high photon energies at which $A = 1 - R_{int}$.

For a symmetrical wafer structure, the absorptivity is given by

$$A(\hbar\omega) = \frac{\left(1-R_{int}(\hbar\omega)\right)\left(1-\mathrm{e}^{-\alpha(\hbar\omega)d}\right)}{1-R_{int}(\hbar\omega)\mathrm{e}^{-\alpha(\hbar\omega)d}} \tag{5}$$

and the absorption coefficient α is determined by

$$\alpha(\hbar\omega) = \frac{\ln\left(\frac{A(\hbar\omega)R_{int}(\hbar\omega)-1+R_{int}(\hbar\omega)}{A(\hbar\omega)-1+R_{int}(\hbar\omega)}\right)}{d}. \tag{6}$$

2.3. Band-to-band recombination coefficient

The radiative band-to-band recombination rate is given by $R = \underline{B}\, np$, where n (p) is the electron (hole) density in the respective band. Here, $\underline{B}$ is the integrated coefficient that is calculated from integrating

$$B(\hbar\omega,T) = \frac{(\hbar\omega)^2 n_r^2}{\pi^2\hbar^3c_0^2}\frac{\alpha(\hbar\omega,T)}{n_i^2(T)}\exp\left(-\frac{\hbar\omega}{kT}\right) \tag{7}$$

with the intrinsic carrier density n_i and refractive index n_r. Eq. (7) is obtained from Eq. (1) and by noting that $np = n_i^2 \exp(\varepsilon_{Fn} - \varepsilon_{Fp}/kT)$, together with the approximation that the 1 in the Bose term can be neglected. It is noted that Eq. (7) was applied in the literature to determine $\underline{B}$ in c-Si, but with some variation in the determined values (see below).

2.4. Applied voltage and quasi-Fermi level splitting

In an ideal diode, it is assumed that there is no transport loss, that the quasi-Fermi level splitting is spatially constant and that the quasi-Fermi level splitting is equal to the applied voltage V_a. In real semiconductor *pn* diodes, transport is determined by the mobilities and lifetimes of charge carriers and governed by the transport equations that involve a gradient of the quasi-Fermi level of each charge carrier type. The transfer of the ideal-diode concepts to the real-diode case is thus questionable, although it has been judged to be applicable to high-efficiency solar-cell diodes, e.g. [7].

For EL, Würfel [3] noted that for a good luminescent *pn* diode $\varepsilon_{Fn} - \varepsilon_{Fp} = \mathrm{e}\, V_a$ and thus from Eq. (3) it follows that

$$j_\gamma(\hbar\omega) = \frac{(\hbar\omega)^2}{4\pi^2\hbar^3c_0^2}A(\hbar\omega)\exp\left(-\frac{\hbar\omega}{kT}\right)\exp\left(\frac{V_a}{kT}\right). \tag{8}$$

Schick *et al.* [5] have related Kirchhoff's generalised law to the applied voltage, taking into account spatially non-constant carrier distributions, and also deduced that the luminescence intensity is proportional to $\exp(eV_a/kT)$.

Fuhs *et al.* [10], assuming that $\varepsilon_{Fn} - \varepsilon_{Fp}$ equals $\mathrm{e}\, V_a$ and together with the current-voltage diode equation, formulated

$$j_\gamma(\hbar\omega) = \frac{j_d}{j_s}\frac{(\hbar\omega)^2}{4\pi^2\hbar^3c_0^2}A(\hbar\omega)\exp\left(-\frac{\hbar\omega}{kT}\right). \tag{9}$$

Here, j_d is the dark current density and j_s is the saturation current density.

2.5. Analytical and numerical modelling

We apply the Shockley theory of transport in *pn* diodes to calculate charge carrier profiles and ε_{Fn} and ε_{Fp} distributions [11,12]. The device modelling programme SC-Simul [13,14] allows one to determine all the physical properties of interest, e.g., the free electron and hole densities and the electrostatic potential, which are the three spatially dependent variables of the transport and device equations. The input parameters are the semiconductor properties for the different layers with which a structure is built, like the band gap E_g, effective densities of states in the band, free carrier mobilities, electron affinity, capture coefficients for defect states and parameters for defect densities and distributions.

3. Experimental

Quantitative PL and EL measurements were performed with a calibrated set-up. The radiation was dispersed by a monochromator and detected by a LN2 cooled InGaAs photodiode. The fraction of the photoluminescence was measured that was emitted to the side from which the samples were excited, e.g., by a near-IR laserdiode.

Crystalline silicon wafers were prepared with high-quality hydrogenated amorphous silicon (a-Si:H) or silicon nitride passivation layers on both sides. Diode structures consisted of a-Si:H/c-Si heterojunction diodes with a-Si:H layer thicknesses between 5 and 30 nm and an Al back contact.

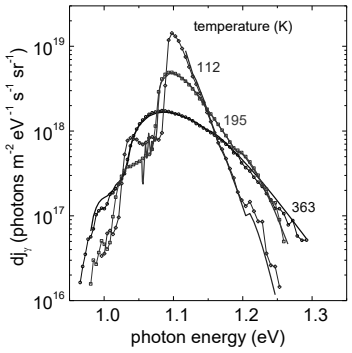

Fig. 1. Temperature dependent photoluminescence spectra of a p-type c-Si wafer. Data points are from the experiment, full lines from theory with the optical absorption coefficient according to Eq. (2).

4. Results and discussion

4.1. Comparison of experimental and analytic photoluminescence spectra

The strategy for the validation of Kirchhoff's generalised law for c-Si consists of the comparison between the experimental and analytical PL spectra of c-Si wafers which were symmetrically passivated with a thin amorphous silicon layer on either side. The analytical spectra were generated from Eq. (2) with input from Eq. (5), for which the absorption coefficient of c-Si determined from the optical transmission measurements by MacFarlane [15] was inserted. Apart from the slightly varying R_{int}, the quasi-Fermi level splitting was the only adjustable parameter for the analytical spectra of Eq. (2). Simulation results have shown that for the excitation conditions in the experiment, the excess carrier distributions were sufficiently homogeneous so that a spatially constant quasi-Fermi level splitting was assumed for Eq. (2).

Fig. 1 shows experimental and analytical spectra for T = 112 K, 195 K and 363 K. The distributions of the experimental spectra are typical for c-Si, showing the phonon-related transitions and a narrowing of the spectral width, together with a band-gap shift, with decreasing temperature.

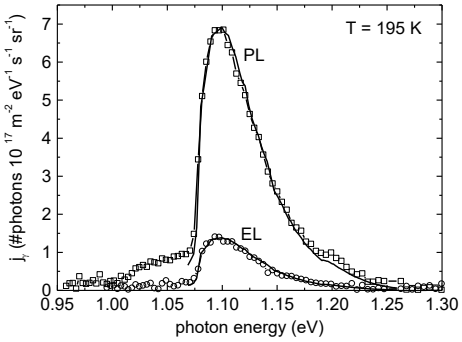

Fig. 2. Experimental and theoretical PL spectrum at open circuit and EL spectrum for an a-Si:H/c-Si diode at 195 K.

The full lines in Fig. 1 were generated with the optical α and Eq. (2). There is good agreement for each T between the experimental and the theoretical curves. We thus have a correct reproduction of the experimental spectra. At a given photon energy, the optical absorption coefficient is related to processes involving, e.g., phonon absorption in the transmission measurement but phonon emission in the luminescence experiment [16].

Fig. 2 shows PL and EL spectra for an (n)a-Si:H/(p)c-Si diode with a 20 nm a-Si:H layer and a 220 µm thick c-Si wafer. Here, the theoretical spectra were generated from Eq. (2) with different interface conditions for the diode structure with its backside mirror-like metal contact compared to the wafer in Fig. 1. The agreement between the theoretical and experimental spectra in Fig. 2 is very good. The same is true for measurements at other T between 112 K and 300 K.

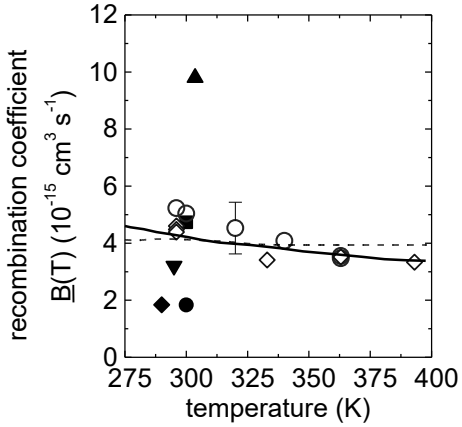

Fig. 3. Band-to-band recombination coefficient vs T. Our results are represented by open symbols (diamonds: a-Si:H passivated wafer, circles: SiN passivated wafer). Full symbols are from the literature (downward triangle [4], square [19], diamond [20], upward triangle [21], circle (22]). The dashed and full curves represent the theoretical variation with different $n_i(T)$, digitised from [23].

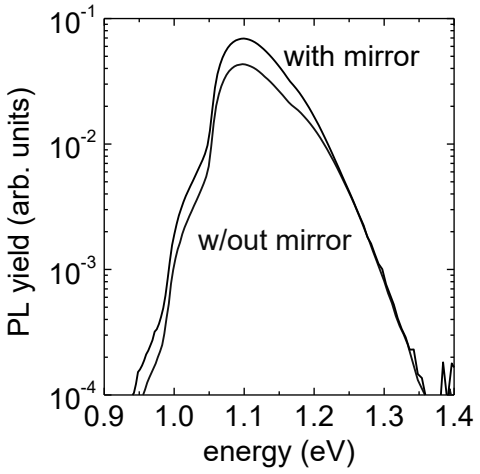

Fig. 4. Influence of back-reflection on the measured photoluminescence of a c-Si wafer at room temperature. A mirror was attached to the back surface in order to change the absorptivity.

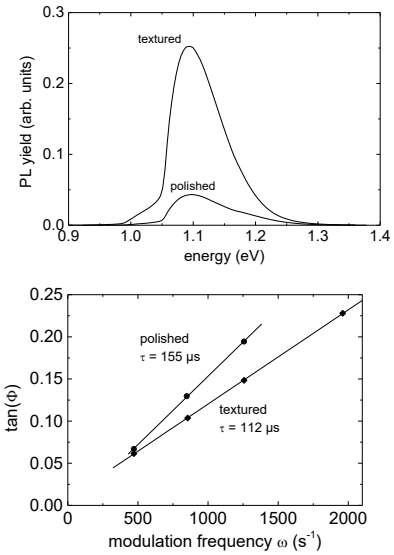

Fig. 5. Influence of texture on the emitted PL (top). The minority carrier non-radiative lifetime was determined by the phase shift of the modulated photoluminescence (bottom).

Both the spectral width and phonon-related features agree in Figs. 1 and 2 for the experimental spectra from wafer structures and diodes and for the theoretical spectra, which were calculated with Eq. (2). We take this agreement as evidence that Kirchhoff's generalised law is valid for the indirect semiconductor crystalline silicon. Our results at different temperatures complement nicely the room-temperature measurements that have shown good agreement between the experimental and theoretical spectra of c-Si [4].

4.2. Determination of the radiative recombination coefficient above room temperature

Fig. 3 shows the T dependence of the band-to-band recombination coefficient for c-Si. Nominally identical wafers were a-Si:H passivated and silicon nitride passivated for the PL measurements. The absorption coefficient for Eq. (7) was determined from Eqs. (4) - (6), i.e., it was determined from quantitative luminescence data. The resulting error bar is sketched in Fig. 3. The T dependence of n_r was calculated after [17], n_i was calculated from the temperature dependence of the band gap [18] for which no shrinking was taken into account because of the moderate excitation conditions.

Full symbols show other experimental results from the literature [19-22]. For a high precision determination of $\underline{B}$, Trupke *et al.* [19] applied relative PL measurements to determine a relative absorption coefficient which was then calibrated with α from optical measurements. Daub [4] also evaluated PL data. The other experimental data points from earlier evaluation [20-22] are included for completeness. The lines are from theoretical approaches which are based on input data for α and different n_i [23]. It can be seen that n_i determines the T dependence to some degree.

In comparison with the other experimental data, the best agreement is found with the room-temperature value determined by Trupke *et al.* [19]. With the results in Fig. 3, the lower T data from [19] for $\underline{B}$ are expanded by another 100 K to higher T, where $\underline{B}$ drops slightly with increasing T.

4.3. Influence of the absorptivity term on the luminescence emission

Eq. (2) implies that the absorptivity term plays an important role for the emission of photons from the sample. The simplified form of A for identical interfaces is given in Eq. (4). If emission to one hemisphere is blocked by a mirror interface, the change in A will change the shape of the emission spectrum. As Fig. 4 indicates, the luminescence yield increases with no change in the quasi-Fermi level splitting which can be seen at higher energies. Here, $A = 1 - R_{front}$ and the luminescence yield is the same because of re-absorption of the photons that are reflected by the back mirror. At lower energies, more photons escape to the front and get collected because re-absorption is reduced. For the peak, the increase in yield is still less than but close to a factor of 2. If this was translated into a change in the minority carrier density or the lifetime, one would also get an error of a factor of about 2, because the minority carrier density and thus the lifetime are the same for both cases. In terms of quasi-Fermi level splitting at room-temperature, the error is $kT \ln 2 = 40$ meV.

Texturing of the surface increases the absorptivity, which results in an increase in luminescence yield [24], without a change in the quasi-Fermi level splitting. Fig. 5 shows the increased PL yield of a textured sample in comparison with a polished sample from the same wafer material. The non-radiative lifetime (Fig. 5) that determines the minority-carrier density was determined by

modulated photoluminescence [25] and was found to be similar. Despite the slightly shorter lifetime of the textured sample, the PL yield is much higher because of increased emissivity/absorptivity due to the rough surfaces, light scattering and the enhancement in coupling out photons from the sample.

The results show that conclusions about minority carrier properties from the evaluation of the peak luminescence of different samples can be susceptible to errors if changes in the absorptivity are not monitored.

4.4. Electroluminescence

Eqs. (8) and (9) suggest that the EL spectral shape should not change with V_a or with j_d. Fig. 6 shows that this is indeed the case for the experimental EL of an (n)a-Si:H/(p)c-Si diode. It is noted that the experimental integrated EL yield varies linearly with j_d, as described in Eq. (9). Similar results are presented in [10].

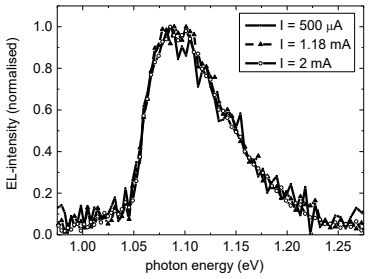

Fig. 6. Good agreement in the spectral shape of the normalised experimental EL spectra of a c-Si heterodiode for current densities that increase by a factor of 2 (T = 296 K).

We apply Eq. (9) to predict the T dependence of the EL yield of a c-Si diode at j_d = 100 mA/cm^2. Fig. 7 shows the analytical spectra with the α from [15] and the assumption that the minority carrier diffusion length is longer than the diode thickness. The yield from the integrated spectra is shown in the inset, and decreases with increasing T. Apart from the T-dependent α, the T-dependence of E_g is the most important variation because it determines j_s and thus also the EL yield. For example, if E_g was taken to be T independent, the EL yield would increase with increasing T.

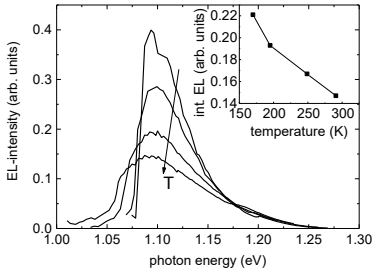

Fig. 7 Analytical electroluminescence spectra after Eq. (9) at a current density of 100 mA/cm². The inset shows the decrease of the integrated electroluminescence with increasing temperature.

In fact, for real diodes Eq. (9) shows that the value of j_s is a limiting factor in achieving a high EL yield. The luminescence efficiency in terms of the quantum efficiency eJ_γ/j_d (J_γ is the integrated flux) at room temperature takes the value 3.6 × 10^{-6} for a 220 µm thick diode with j_s = 2.64 pA/cm^2. If j_s takes the optimum low value of about 10 fA/cm^2, the quantum efficiency increases to 9.5 × 10^{-4}.

As the open-circuit voltage of solar cells also depends on j_s it is tempting to re-write Eq. (9) with the current-voltage relation and the short-circuit current density j_{sc} to read

$$j_\gamma(\hbar\omega) = \frac{j_d \exp\left(\frac{V_{oc}}{kT}\right)}{j_{sc}} \frac{(\hbar\omega)^2}{4\pi^2\hbar^3 c_0^2} A(\hbar\omega) \exp\left(-\frac{\hbar\omega}{kT}\right)$$

i.e., cells with high V_{oc} also show a high EL yield.

The experimental results by Fuhs *et al.* [10] indicate such a correlation, whereas the photovoltaic efficiency in contrast may also be determined and limited by the fill-factor.

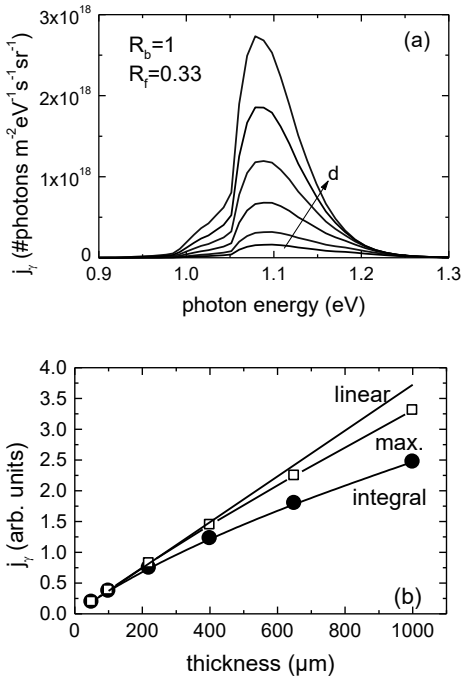

Fig. 8 Analytical EL spectra at 300 K for different diode thicknesses after Eq. (9) at a current density of 0.1 A/cm² (a). The EL maximum and the integrated EL yield increase sub-linearly with increasing thickness because of re-absorption (b).

Increasing the diode thickness results in an increase in the EL yield (Fig. 8(a)). However, re-absorption of luminescent photons becomes more important for thicker diodes. The open symbols in Fig. 8(b) show the relative increase of the maximum EL yield at the peak energy, while the full line indicates the increase in yield if it was linearly related to the diode thickness.

Re-absorption leads to a sub-linear increase of the integrated luminescence yield with increasing thickness, as illustrated by the full circles in Fig. 8(b). Doubling the diode thickness from 200 µm to 400 µm results in an increase in EL efficiency by a factor of about 1.6.

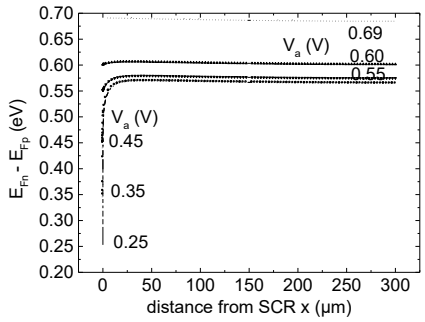

Fig. 9. Analytical solutions of the quasi-Fermi level splitting in a pn diode for different applied voltages. The edge of the space-charge region (SCR) is at x=0.

The analytical results show that only the low-energy photons do not suffer re-absorption - in the range in which A is proportional to αd the EL yield scales linearly with thickness. For the higher photon energies at which A approximates to $(1\text{-}R_{front})$, the EL yield becomes independent of d. A better strategy to further enhance the EL yield is to increase A by texturing and maintaining small values of j_s [24].

4.5. Applied voltage and quasi-Fermi level splitting

In devices like *pn* diodes, the excess carrier profiles depend on the transport equations, on the boundary conditions imposed by extraction at the junction or by the loss by back-contact recombination of minority carriers and on the photogeneration rate.

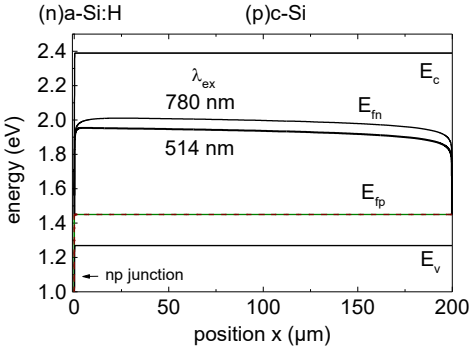

Fig. 10. Numerical solution of the conduction and valence band edges, E_c and E_v, and the quasi-Fermi levels at short circuit in an (n)a-Si:H/(p)c-Si diode for different excitations at 300 K.

Figure 9 depicts the quasi-Fermi level splittings of a *pn* diode under illumination with monochromatic light at different V_a and at T = 300 K. The distributions were calculated with the Shockley theory [11,12] and typical values for crystalline silicon, assuming a diffusion length of 400 µm and α of 1000 cm^{-1}.

It is clear that the applied voltage is not an image of the quasi-Fermi level splitting in the volume of the diode. Closer inspection, as a consequence of the Shockley theory, shows that only at $x = 0$ does the relation $\varepsilon_{Fn} - \varepsilon_{Fp} = e\,V_a$ hold. From the PL evaluation, the quasi-Fermi level splitting in the volume of the wafer will be determined, with the result that $\varepsilon_{Fn} - \varepsilon_{Fp} \geq e\,V_a$. The equality holds at voltages around open-circuit.

Figure 10 shows the full numerical solution with SC-Simul for the quasi-Fermi level splitting at short circuit for an (n)a-Si:H/(p)c-Si diode. The wavelengths of the excitation light were 514 nm and 780 nm and the short-circuit current was the same. This diode had an Ohmic back contact, so that the gradient of ε_{Fn} indicates the net electron flow to the right where carriers are lost. The gradient in ε_{Fp} is too small to be identified in the graph but it drives the hole current, which is much larger than the electron current in the volume of the diode.

To conclude, there is a significant amount of quasi-Fermi level splitting, even though $V_a = 0$.

The results here are similar to the case for AM1.5 illumination in [26] and it is noted that PL, measured at short circuit and at open circuit, allows an analysis of the interface quality of such (n)a-Si:H/(p)c-Si diodes [26].

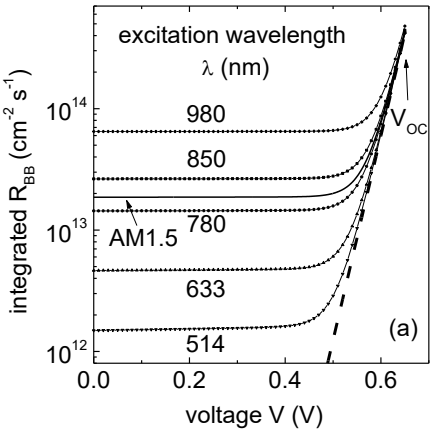

Fig. 11. Spatially integrated band-to-band recombination rate in an (n)a-Si:H/(p)c-Si diode. The dashed straight line indicates the recombination rate that would result if $\varepsilon_{Fn} - \varepsilon_{Fp}$ equalled $e\,V_a$.

The numerical results in Fig. 10 nicely complement the analytical results in Fig. 9. There is a substantial amount of quasi-Fermi level splitting in Fig. 9, independent of the applied voltage. The typical radiative band-to-band recombination rates as a function of voltage are shown in Fig. 11. Indeed, the numerical results for different excitation conditions show the independence of the radiative recombination rate on voltage for quite a wide voltage range. The full straight line in Fig. 11 indicates

how the radiative recombination rate would drop if the relation $\varepsilon_{Fn} - \varepsilon_{Fp} = e\, V_a$ was valid.

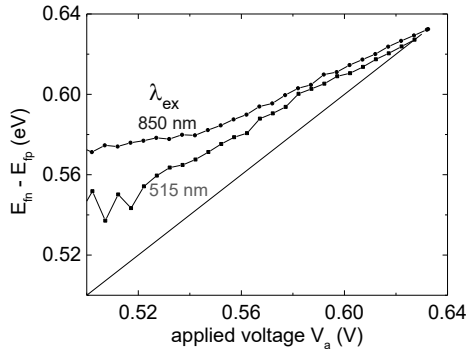

Fig. 12. Experimentally determined $\varepsilon_{Fn} - \varepsilon_{Fp}$ vs. applied voltage for a commercial c-Si pn diode and for two excitation wavelengths. The straight line represents the diagonal.

Fig. 12 shows results from experimental PL, collected from a commercial c-Si *pn* diode at different applied voltages. For calibration, $\varepsilon_{Fn} - \varepsilon_{Fp}$ was set equal to e V_{oc} at open circuit. The diagonal is the prediction from the ideal-diode model. As predicted by the simulation in Fig. 11, the deduced quasi-Fermi level splitting is larger than expected from V_a. Construction of a current-voltage curve by adjusting the voltage scale from PL data thus may lead to errors if $(\varepsilon_{Fn} - \varepsilon_{Fp})$/e is set equal to V_a.

5. Conclusions

For wafer and diode structures, we have confirmed Kirchhoff's generalised law for c-Si and have corroborated earlier results that it is also valid for indirect semiconductors. It is necessary to properly take into account the absorptivity term in the analysis of the luminescence radiation from a device structure. We have determined $\underline{B}$ in the T range between room temperature and 393 K and estimated the T of the EL efficiency. The relation between V_a and $\varepsilon_{Fn} - \varepsilon_{Fp}$ cannot be transferred from ideal diode to real diode structures. We identified by application of the Shockley theory for illuminated *pn* diodes and by numerical modelling that typically $\varepsilon_{Fn} - \varepsilon_{Fp} \geq e\, V_a$ at lower voltages.

Acknowledgements

The authors thank G. H. Bauer for support and discussions. Provision of samples by colleagues from ISE, Gelsenkirchen and HMI, Berlin, within a BMBF (Berlin) funded project, is gratefully acknowledged.

References

[1] G. Lasher, F. Stern, Phys. Rev. **133**, A553 (1964).
[2] R.B. Stephens, Phys. Rev. B **29**, 3283 (1984).
[3] P. Würfel, J. Phys. C **15**, 3967 (1982)
[4] E. Daub, Thesis, Universität Karlsruhe (1995).
[5] K. Schick, E. Daub, S. Finkbeiner, P. Würfel, Appl. Phys. A **54**, 109 (1992).
[6] T. Tiedje. E. Yablonovitch, G.D. Cody, B.G. Brooks, IEEE Trans. ED **31**, 711 (1984).
[7] T. Trupke, R. A. Bardos, M. D. Abbott, J. E. Cotter, Appl. Phys. Lett. **87**, 093503 (2005).
[8] G. Lucovsky, A.J. Varga, R.F. Schwarz, Solid State Comm. **3**, 9 (1965).
[9] E. Daub, P. Würfel, Phys. Rev. Lett. **74**, 1020 (1995).
[10] W. Fuhs, A. Laades, K. von Maydell, O.B. Gusev, E. Terukov, S. Kazitsyna-Baranovski, G. Weiser, J. Non-Cryst. Solids **352**, 1884 (2006).
[11] H. J. Hovel, Solar Cells (Academic Press, New York, 1975).
[12] H. G. Wagemann, H. Eschrich, Grundlagen der photovoltaischen Energiewandlung (Teubner, Stuttgart, 1994).
[13] R. Brüggemann, M. Rösch, J. Optoelectron. Adv. Mater. **7**, 65 (2005).
[14] M. Rösch, T. Unold, R. Pointmayer, G.H. Bauer, MRS. Symp. Proc. **557**, 463 (2000).
[15] G.G. MacFarlane, T.P. McLean, J.E. Quarrington, V. Roberts, Phys. Rev. **111**, 1245 (1958).
[16] P. Würfel, S. Finkbeiner, E. Daub, Appl. Phys. A **60**, 67 (1995).
[17] G. E. Jellison, F.A. Modine, J. Appl. Phys. **76**, 3758 (1994).
[18] W. Bludau, A. Onton, W. Heinke, J. Appl. Phys. **45**, 1846 (1974).
[19] T. Trupke, M.A. Green, P. Würfel, P.P. Altermatt, A. Wang, J. Zhao, J. Appl. Phys. **94**, 4930 (2003).
[20] Y.P. Varshni, Phys. Status Solidi **19**, 459 (1967).
[21] H. Schlangenotto, H. Maeder, W. Gerlach, Phys. Status Solidi (a) **21**, 357 (1974).
[22] W. Michaelis, M.H. Pilkuhn, Phys. Status Solidi **36**, 311 (1969).
[23] M. Ruff, M. Fick, R. Lindner, U. Rössler, R. Helbig, J. Appl. Phys. **74**, 267 (1993).
[24] M.A. Green, J. Zhao, A. Wang, P.J. Reece, M. Gal, Nature **412**, 805 (2001).
[25] R. Brüggemann, S. Reynolds, J. Non-Cryst. Solids **352**, 1888 (2006).
[26] G. H. Bauer, R. Brüggemann, M. Rösch, S. Tardon, T. Unold, Phys. Status Solidi (c) **1**, 1308 (2004).

*Corresponding author: rudi.brueggemann@uni-oldenburg.de